16

Electromagnetic Response of Extraordinary Transmission Plates Inspired on Babinet's Principle

Miguel Navarro-Cía, Miguel Beruete and Mario Sorolla
Millimetre and Terahertz Waves Laboratory, Universidad Pública de Navarra
Spain

1. Introduction

This chapter is devoted to polarization effects arisen from perforated metallic plates exhibiting extraordinary transmission (ET). Setting aside the state-of-the-art of perforated metallic plates, we show that by applying Babinet's principle, subwavelength hole arrays (SHAs) arranged in rectangular lattice can further enhance its potential polarization response. Different perspectives are brought about to describe and understand the particular behaviour of self-complementariness-based SHAs: Babinet's principle, equivalent circuit analysis, retrieved constitutive parameters, etc. Afterwards, we embark on the numerical analysis of stacked self-complementariness-based perforated plates. It is shown the potential of having a birefringent artificial medium behaving like negative and positive effective refractive index for the vertical and horizontal polarization, respectively. All these findings are experimentally demonstrated at millimetre-waves.

2. Background

Since the ending of the Second World War, the electromagnetic (EM) properties of artificial materials (dielectric and magnetic) have been studied by both physics and engineering communities (Collin, 1991). Unlike traditional materials, these man-made composites achieve their EM properties by directly manipulating EM waves, yielding to frequency selective behaviours. This property has a great practical consequence since it is the operative foundation of a wide range of devices such as filters, signal couplers, radiation elements, etc.

2.1 Classical perforated plates: dichroic filters

The analysis of light transmission through holes or gratings has a long history, tracing back to the beginning of the 20th century (Rayleigh, 1907; Synge, 1928; Wood, 1902). However, perforated plates had their golden years in the 50s, 60s and 70s in microwave engineering (Brown, 1953; Chen 1971, 1973; Robinson, 1960) and infrared (Ulrich 1967), when they were exploited as frequency selective surfaces/filters (FSSs) and their 100% transmittance at wavelengths slightly above the period was discussed. All the FSSs considered at that time had aperture sizes considerably large for those frequencies at which there was transmittance, see Fig. 1(left). The principle of operation of those FSSs called dichroic filters

is excellently described in (Goldsmith, 1998), where the analysis is discussed under the transmission line formalism (Fig. 1.1(right)): The waveguide defined by the hole is represented as a series admittance Y and the discontinuities between the guide and free-space are modelled with shunt admittances Y_s at each end of the perforated plate. Needless to say, the free-space is represented by shunt admittances Y_{fs}. Nevertheless, this approach inherently ignores diffraction (thus, the in-plane period must be small enough relative to the operating wavelength). As it was pointed out in (Beruete et al., 2006b), this restriction is of major importance in the description of extraordinary transmission phenomena.

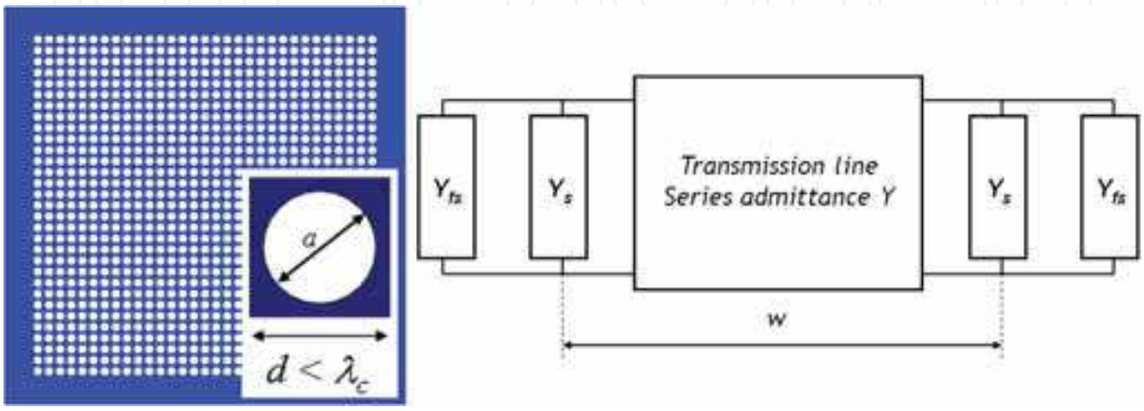

Fig. 1. (left) Schematic of a classical frequency selective surface. Inset: unit cell. (right) Transmission line model to analyse the frequency response of this kind of perforated plates. The length of the waveguide, that is, the plate thickness is denoted as w

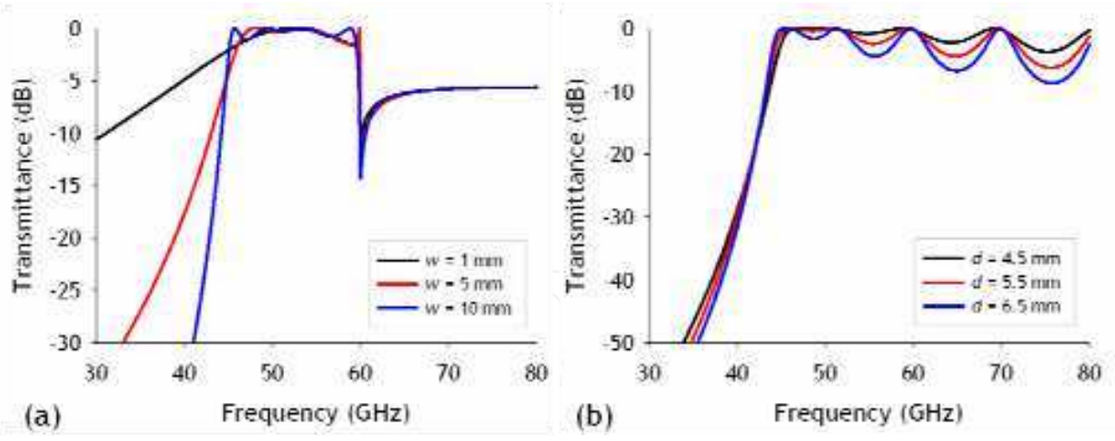

Fig. 2. Frequency response of a dichroic filter with hole diameter a = 4 mm: (a) and in-plane lattice constant d = 5 mm as a function of the waveguide length w = 1, 5 and 10 mm; (b) idem with metal thickness w = 10 mm as a function of the in-plane lattice constant d = 4.5, 5.5 and 6.5 mm applying the equivalent circuit proposed in (Goldsmith, 1998). Note that the Wood's anomaly is not captured with the equivalent circuit

In short, the main features of these dichroic filters are (see Fig. 2):

- The lower limit of the fundamental transmission frequency band is determined by the cut-off frequency of the waveguide defined by the hole, whereas the higher cut-off

frequency is governed by the periodicity (Hessel & Oliner, 1965; Rayleigh, 1907; Wood, 1902). At that particular wavelength, a diffracted order that previously contained energy becomes imaginary (goes evanescent), and, for a perfectly conducting grating, the law of conservation of energy demands that the energy previously contained in that order be redistributed among the other remaining diffracted orders.

- The period of the ripples within the passband decreases as the plate thickness increases, because of the increment of electrical length between the guide – free-space discontinuities.
- Also, the longer the plate thickness, the steeper the rise from total reflection to transmission at the lower frequency.
- The larger the in-plane periodicity, the higher the ripple within the passband because the shunt reactance Y_s increases.

Because of the last property, the holes were densely packed at that time (ripple is undesired for technological applications) and this may be one of the reasons of the ignorance of the ET in the electrical engineering community.

2.2 Overcoming Bethe-Bouwkamp's theoretical model

In 1940s Bethe developed a deep study of the field scattered by a single aperture on a thin opaque (perfect electric conductor - PEC) screen by considering it as a magnetic dipole parallel to the screen along with an electric dipole perpendicular to it (the latter one is only required for oblique incidence) (Bethe, 1944). Notice that parallel electric dipoles and perpendicular magnetic dipoles are prohibited by the boundary conditions that impose the parallel electric field and the perpendicular magnetic field to vanish at a perfect electric conductor. He showed that under normal incidence and assuming that the incident intensity is constant over the area of the hole, the transmittance is proportional to $(r/\lambda)^4$ where r is the hole radius. This factor implies extremely low transmission for subwavelength holes. Subsequently, higher-order analytical corrections were introduced by Bouwkamp (Bouwkamp, 1950, 1950b, 1954).

The discovery in 1998 of enhanced light transmission compared to Bethe-Bouwkamp's model in silver plates perforated with periodic subwavelength hole arrays, see Fig. 3(a), launched the field of extraordinary optical transmission (EOT). However, there are signs indicating that the effect was actually discovered during the development of the near-field scanning optical microscopy (NSOM) (Betzig et al., 1986). In 1928 Synge proposed the use of a small aperture close to a sample surface to overcome the diffraction limit imposed by the fact that the propagating waves are limited to $k_x^2 + k_y^2 < (\omega/c)^2$ and thus, the maximum resolution in the image cannot be greater than $\Delta \approx 2\pi/k_{max} = 2\pi c/\omega = \lambda$ (Synge, 1928). This approach was reused by Betzig *et al.* who designed, characterized and implemented hole arrays for the NSOM. During the arrays characterization, transmittance overcoming Bethe's model was observed and tentatively attributed the observation to surface plasmons with no further analysis (Betzig, 1988): "*From the lower graph in Fig. 3.9 it is clear that a significant amount of visible light can be passed through apertures almost as small as λ/10 in diameter, (...) This may once again be a consequence of the finite conductivity and opacity of the screen, or some other phenomenon may be involved which enhances the transport of radiation (e.g. the existence of surface plasmon within the aperture). (...) This provides further circumstantial evidence for hypothesis that some unknown phenomenon is responsible for the high transmission coefficients for the smaller apertures.*"

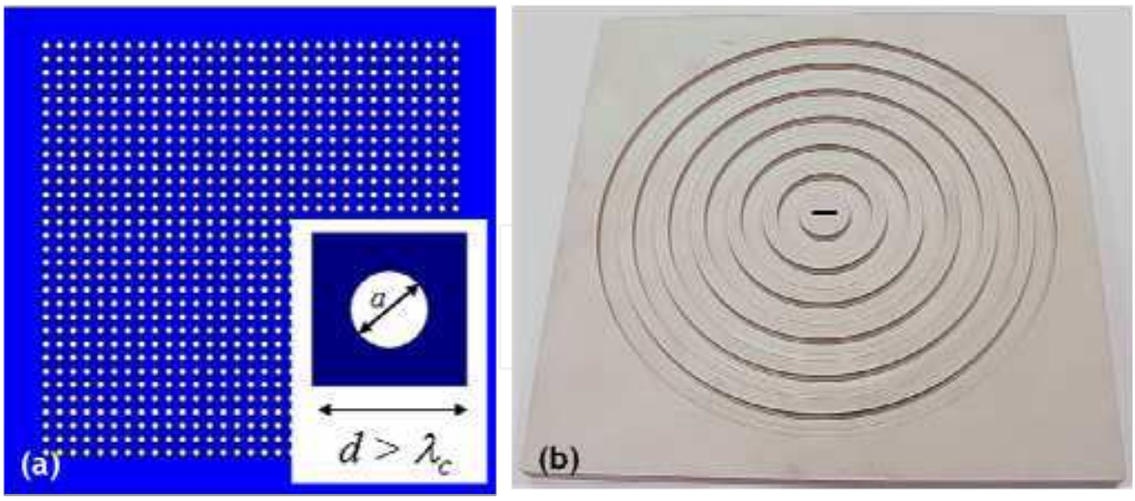

Fig. 3. (a) Schematic of subwavelength hole arrays. Inset: unit cell. (b) Prototype of a slot surrounded by concentric corrugations (Bull's eye configuration)

Nevertheless, it is true that the field took off with Ebbessen and co-workers' deep analyses which brought both theory and experiments to bear on the remarkable conclusion that transmission is mediated via SPPs.

Countless papers followed Ebbesen's seminal paper calling some of them the SPP hypothesis into question or giving other perspectives to the underlying physics of the EOT. Firstly, because of its simplicity, theoretical analyses considered the one-dimensional grating: a periodic array of slits (Porto et al., 1999; Schröter & Heitmann, 1998; Treacy, 1999, 2002). All these works showed that one-dimensional gratings have efficient channels for light transmission because of the non-cut-off slit waveguide that do not exist for hole arrays, so the SPPs theory of one-dimensional slits (although interesting) might not be useful for explaining EOT effect on SHAs.

Subsequently, researchers embarked on the study of the underlying physics of the bigrating. The main works, from the point of view of these authors, are gathered together in the following points according to the different theses proposed.

The first mechanism proposed was the interaction of the apertures with surface plasmons (Barnes et al., 2004; Degiron et al., 2002; Ebbesen et al., 1998; Ghaemi et al. 1998; Krishnan et al., 2001; Martín-Moreno et al., 2001; Salomon et al., 2001). The work of Ebbesen *et al.* was mainly devoted to experimentally study the influence of Wood's anomaly (but not linking it with the resonant peak) (Ghaemi et al. 1998), the dielectric environment (Krishnan et al., 2001), the hole depth (Degiron et al., 2002) and the angle of incidence (Barnes et al., 2004) so as to support their hypothesis based on SPPs. On the other hand, Martín-Moreno, García-Vidal and colleagues (Martín-Moreno et al., 2001) presented a rigorous theory (minimal model) that considered SPPs on infinite grids coupled through an evanescent mode(s) of the hole. Similar line of reasoning was also followed by Salomon *et al.* (Salomon et al., 2001) who presented a near-field picture of the holes to highlight the SPPs Bloch waves as well. Martín-Moreno *et al.* only modelled the response at normal incidence and captured many (but not all) of the prominent features of the experimental results. The minimal model is based on the multiple scattering formalism and assumes the imaginary part of the electric permittivity of the metal $\varepsilon_i = 0$, i.e. no absorption, and one fundamental mode, the least decaying mode

inside the subwavelength hole (if the hole is circular, it is the TE_{11}). The main counterintuitive results is that the reflection amplitude is larger than unity at the resonance, but it is explained because the fundamental mode inside the hole is evanescent, for which current conservation only restricts that the imaginary part of the reflection coefficient must be equal or greater than 0, with no constraint on the real part of it. This fact lets the zeroth order transmission coefficient achieve arbitrarily high values. An extension of this model that accounts for the penetration of the EM waves into metals at higher frequencies considers surface impedance boundary conditions (J.D. Jackson, 1999) on the metal-interfaces defining the metal film (but not inside the hole) (Martín-Moreno et al., 2001). An unforeseen consequence of the model of Martín-Moreno *et al.* is that the results may allow EOT in any frequency range because of the PEC boundary conditions (this fact makes all lengths involved in the system scalable), even at frequencies such as microwaves or millimetre-waves (Beruete et al., 2004) where SPPs make no sense. Thus, despite they were still discussing about SPPs, their work was another proof that the physics underlying the mechanism of enhanced transmission through SHAs is more complicated. Needless to say, although all these works are founded on SPPs, they are also considering the periodicity as an important ingredient because the dispersion diagram of SPP has no discontinuities if the interface is smooth. However, when a periodic perforation/corrugation is introduced along the interface, the dispersion relation shows band structure and energy gaps that allow phase-matching between the incident light and the SPPs.

Other mechanism proposed was dynamical light diffraction and Wood's anomaly (García-de-Abajo et al., 2005; Genet et al., 2003; D.R. Jackson et al., 2005; Lezec & Thio, 2004; Lomakin et al., 2004, 2005; Sarrazin et al., 2003, 2005). Genet *et al.* and Sarrazin *et al.* stressed the role of multiple-scattering paths. However, the former emphasized their work on resonant and nonresonant mechanisms from Fano (Fano, 1941) perspective (Genet *et al.*, 2003), whereas the latter devoted their study on Wood's anomalies which are intrinsically related to periodic structures (Sarrazin et al., 2003), and afterwards to Brewster-Zenneck modes (Sarrazin 2005). EOT on nonmetallic systems gave cause for introducing a new model based on interference of diffracted evanescent waves generated by subwavelength marks at the surface of the screen, leading to transmission suppression as well as enhancement (Lezec & Thio, 2004). Babinet's principle was used by García de Abajo and co-workers in order to study light transmission through hole arrays in PEC thin films by relating it to the reflection on planar arrays of metallic disks, which are solved from the multipolar polarizability of single disks (García-de-Abajo et al., 2005). Finally, Jackson *et al.* (D.R. Jackson et al., 2005) and Lomakin *et al.* (Lomakin et al., 2004, 2005) focused their effort on leaky waves formalism and Wood's anomalies (Hessel & Oliner, 1965). Remarkable of this approach is that it gives explanation for any frequency range, which instead of relying on SPPs, it points out the relevance of the periodicity and the surface waves regardless of their exact nature: leaky SPPs (optics) or leaky waves (microwaves and millimetre-waves). Needless to say, it does not account unfortunately for the potential coupling between surface waves of each interface through the metal in layers whose thickness is smaller than the skin depth as it may happen in optics. It is worth recalling that Ulrich already studied hole arrays under the perspective of surface waves, although the meshes were composed of dense-packed holes like the FSSs shown before (Ulrich & Tacke, 1972, 1974).

To bridge the gap between both theories, Pendry *et al.* captured the physics of EOT on SHAs in a unified theoretical framework called spoof surface plasmon (García-Vidal et al., 2005;

Pendry et al., 2004). However, the importance of this theory was not the mimicked response of SPPs by surface waves in PEC screens because this is already implicit in the dynamical diffraction formalism (leaky waves) – and in classical books of microwave engineering (Collin, 1991) –, but to apply the homogenization theory to show that the effective dielectric function of mesoscopic SHAs and SSAs structures resembles a Drude model, whose plasma frequency can be engineered via the geometry of the holes/corrugations alone, allowing the excitation of SPPs-like states in any region of the spectrum where the PEC condition approximates the metallic response.

Despite their differences, the shared line of reasoning of all theories presented before is that the phase-matching of the incident radiation to a surface wave provided by the periodicity is crucial for transmission enhancement via evanescent tunnelling. Therefore, the same process may arise for a single aperture surrounded by a regular array of corrugations (Fig. 3(b)) (Beruete et al., 2004b, 2005; García-Vidal et al., 2003; Grupp et al., 1999; D.R. Jackson, 2005; Lezec et al., 2002; Thio et al., 2001, 2002).

EOT is still a subject of debate, but after clarifying the limits of each theory, all seem to be in perfect agreement with experiment. In addition, equivalent circuit models have emerged that explain the phenomenon from an engineering point of view (Beruete et al., 2011; Medina et al., 2008). This theory is based on the concept of impedance matching model which predicts enhanced transmission in systems that are not periodic at all and where SPPs are not even defined. Remarkable is that it has been experimentally validated in circular waveguide environment with an off-centred diaphragms (Medina et al., 2009). Thus, this is another theory to add to all that have been already proposed to explain the really complex physics of EOT (or ET at frequencies different than visible).

2.3 Stacked subwavelength hole arrays for negative refractive index metamaterials: fishnet-like structure

Some particular relationships among the phenomena electromagnetic/photonic band-gaps, ET and negative refraction were proposed in the past years, i.e., photonic crystals exhibit negative refraction effects (Notomi, 2002) and electromagnetic and photonic band gaps have been reported in SSHAs (Ye & Zhang, 2005). Soon after, the first fabrication and experimental verification of a holey metal-dielectric-metal structure exhibiting a negative refractive index around 2 microns was reported (Zhang et al., 2005b). A numerical demonstration of the negative index of refraction achievable with this structure was presented in (Zhang et al., 2005). Similar results were published in (Dolling et al., 2006).

The full connection among the three phenomena was shown subsequently with periodically stacked metallic plates perforated with SHAs to form a structure showing backward wave propagation within the ET regime (Beruete et al., 2006). It has to be noted that the in-plane periodicity is of the order of free space wavelength, but it is the longitudinal periodicity which determines the kind of propagation. Given the subwavelength stacking essential to achieve backward propagation, the structure can be homogenized along the longitudinal dimension, allowing the use of the metamaterial term in this dimension. This is the key difference between the ET metamaterial (ETM) and the backward propagation observed in standard PBGs (Notomi, 2002) where it takes place above the forbidden frequency gap with a lattice constant to free space wavelength ratio larger than 0.5. On the other hand, the ETM is apparently similar to the realizations of (Zhang et al., 2005b) and (Dolling et al., 2006). Nevertheless, the key difference is that the ETM introduced by Beruete *et al.* (Beruete et al.,

2006) is a real tuneable EBG comprising several periods, whereas the structures presented in (Dolling et al., 2006; Zhang et al., 2005b) consist of an isolated period which cannot account for Floquet-Bloch framework. Moreover, one of the drawbacks of such structures (Dolling et al., 2006; Zhang et al., 2005b) is that they suffer from losses, even for its minimal size structure due to the operating wavelength. The conductor losses are relevant at optical frequencies but not so important at millimetre-waves or even in the infrared. Dielectric losses are less relevant and can be overcome by using air as a dielectric insulator provided membranes are employed as described in (Beruete et al., 2006). Thus, regarding conducting and dielectric losses, not only the free-standing ETM is more advantageous, but also because it is optimized in terms of ET to enhance transmission unlike (Dolling et al., 2006; Zhang et al., 2005b). Recently, magnetic photonic crystals constructed from periodic arrangements of available (possibly anisotropic) homogeneous material layers have been proposed. These structures can exhibit the phenomena of minimal reflection at their interface, large amplitude growth of the harmonic wave within the crystal, and concurrent group velocity slow-down (Mumcu et al., 2006).

3. Babinet's principle, complementariness, and self-complementariness

Prior to any analysis of some curious polarization effects presented here in modified SHAs, we require clarifying some concepts. Let us start with the meaning of complementariness for this work. Consider a free-standing thin metallic screen with air inclusions as sketched on the left-hand side of Fig. 4. The complementary structure is the one shown on the right, where the metallic part has been substituted by air and the apertures by metallic parts. The mathematical description of this concept is fairly simple: if one denotes S_a the set of apertures (and obstructions) on the left, and S_b the one of the right, their union is the completely obstructing surface $S = S_a + S_b$.

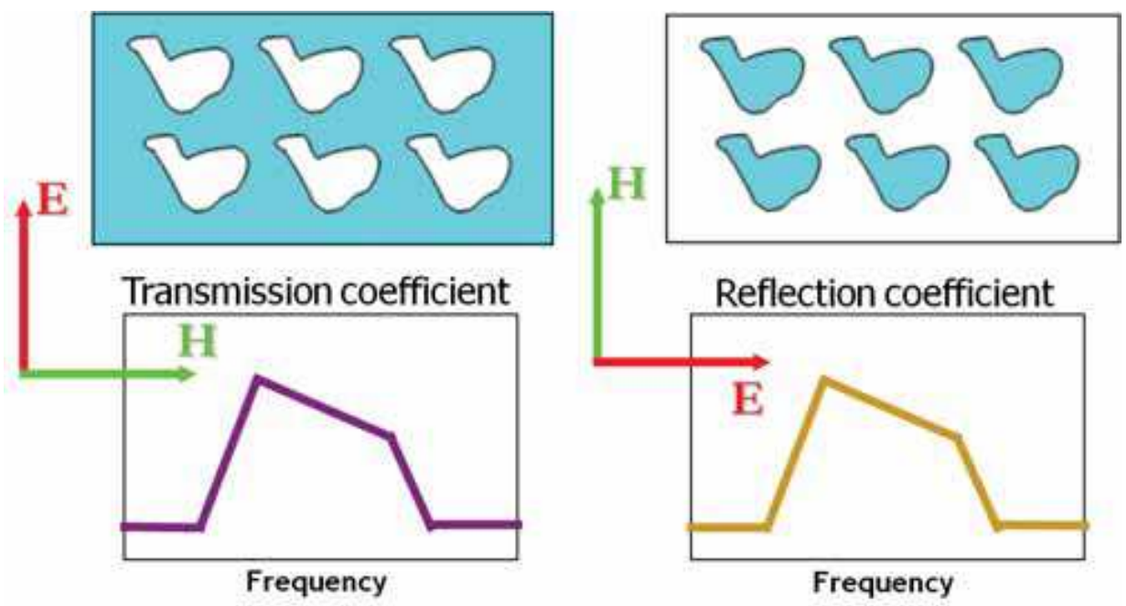

Fig. 4. Example of complementary screens (top sketches) and their electromagnetic response (bottom spectra)

An extension of this idea is the self-complementariness. In this case, the layer has a metal zone congruent to the open area, i.e. the two areas coincide by shift. Thus, the structure is intrinsically composed of its complementary topology, see Fig. 5.
Closely related to the previous concepts, there is an important and common used principle in optics, antenna field and also in metamaterials (Falcone et al., 2004) which establishes the relationship between the diffraction fields of complementary perfectly conducting ($\sigma \to \infty$) infinitely thin ($t \to 0$) screens of infinite extent: the Babinet's principle (Born & Wolf, 1999), (Ishimaru, 1990), (Jackson, 1999). This principle states that the sum of the diffraction fields U_{Sa} and U_{Sb} behind two complementary screens, S_a and S_b, is the field U_0 observed without diffraction objects:

$$U_0 = U_{Sa} + U_{Sb} \tag{1}$$

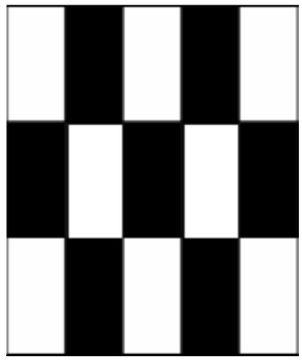

Fig. 5. Example of self-complementary structure

Rewriting this principle more conveniently for our purposes in terms of electric and magnetic fields, it can be read as follows: if $F = (E, H)$ is the solution of S_a, then $F'(E', H') = (-(\mu/\varepsilon)^{1/2} \cdot H, (\varepsilon/\mu)^{1/2} \cdot E)$ is the solution of S_b. This is indeed nothing but the connection between the reflected fields of S_b for a given polarization with the transmitted fields of S_a, which in plain words says that the reflectance spectra of S_b are identical with the transmittance spectra of S_a, see bottom of Fig. 4, and the other way around.

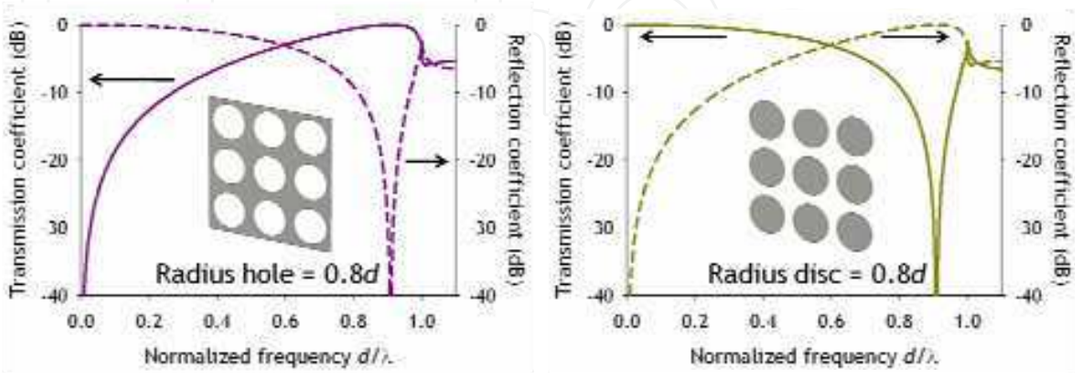

Fig. 6. Scattering parameters in logarithm scale of hole (left) and disk arrays (right) under vertically polarized illumination. (solid line) Transmission coefficient and (dashed line) reflection coefficient

To put this pedagogically in an example within the context of the topic of the chapter, let us show the response of hole and disk arrays infinitely extended transversally and illuminated by a plane-wave under normal incidence. These results have been obtained numerically by the commercial software CST Microwave Studio™. This example will make it easier the description and understanding of the perfect linear polarizer of next section. As Fig. 6 displays, the complementariness of the two structures is completely satisfied in terms of transmission and reflection. Notice how the transmission coefficient of one is the reflection coefficient of the other and the other way around.
If we now take a step further and apply Babinet's principle to a self-complementary screen like the one shown in Fig. 5, we can immediately realize that in the same screen we have both EM responses shown at the bottom of Fig. 4, and thus, a linear polarizer is successfully achieved since for a given polarization there is high transmittance within a certain frequency range, whereas for its orthogonal, there is high reflectance within the same bandwidth.

4. Self-complementary extraordinary transmission layer: perfect linear polarizer

So far, we have given a description of arbitrary screens, but the Babinet's principle may hold evidently for SHAs (Beruete et al., 2007c) such as the doubly periodic arrangement shown in Fig. 7(a). Indeed, by a slight modification of the doubly periodic SHAs, a self-complementary screen is achievable, see Fig. 7(b) where $d_x = a + s$ and $d_y = 2a$ (to fulfil the self-complementary criterion), which should exhibit the linear polarization response described in the previous paragraph. This assumption is confirmed in Fig. 8, where transmittance and reflectance of both SHAs and self-complementary SHAs alongside the SSAs case are plotted. These results have been generated by CST Microwave Studio™ where $s = 0.04d_y$ (needless to say, $d_x = 0.54d_y$, $a = d_y/2$, t infinitely thin and metal modelled as PEC) and we have considered a subwavelength array of slits and holes with or without slits with the periodicity in the x-direction and extending all the way in the y-direction. The remaining z-direction is perpendicular to the plane of array. Apart from the clear self-complementariness of the EM response of the modified SHAs (notice this fact in both transmission and reflection), prominent in Fig. 8(a) is that the transmittance for vertical polarization (E_y) remains unaltered when narrow vertical slits connecting holes are included in the SHAs (note that the solid red trace of Fig. 8(a) is superimposed to the solid black one), whereas the transmittance of the orthogonal polarization (E_x) suffers a strong modification in order to accommodate itself to the self-complementariness principle.
That the vertical polarization remains unaltered by the inclusion of the subwavelength slits may be the manifestation that the current distribution in the vicinity of the hole responsible for the ET suffers no perturbation. Let us then compare the current distribution of simple SHAs and self-complementary ones. As we have already pointed out in this text, the ET is a self-resonance of the hole array, which can be modelled as an LC tank (Beruete et al., 2006; Medina et al., 2008; Ulrich, 1967) and has inductive character for large λ, hence transmittance is negligible when $\lambda \rightarrow \infty$ [see solid red trace of Fig. 8(a)]. Besides, the inset of Fig. 8(a) reinforces the statement about the inductive character of hole arrays in the very subwavelength regime since the phase for vertical polarization tends to + 90 deg as the SSAs (well-known inductive grid) do. Notice in Fig. 9(a) how the conduction currents at ET, which are the main contribution to the inductance – the inductance and the capacitance are

balanced, at least in a first order approach (Ulrich, 1967), at the resonance peak –, are concentrated in the narrow wire between holes. Moreover, the current lines rendered in Fig. 9(a) are closed through displacement currents connecting the upper and lower sides of the hole. This description keeps valid when a narrow vertical slit is introduced connecting consecutive holes [see Fig. 7(b) and Fig. 9(b)], and thus, the assumption pointed out at the beginning of the paragraph is confirmed.

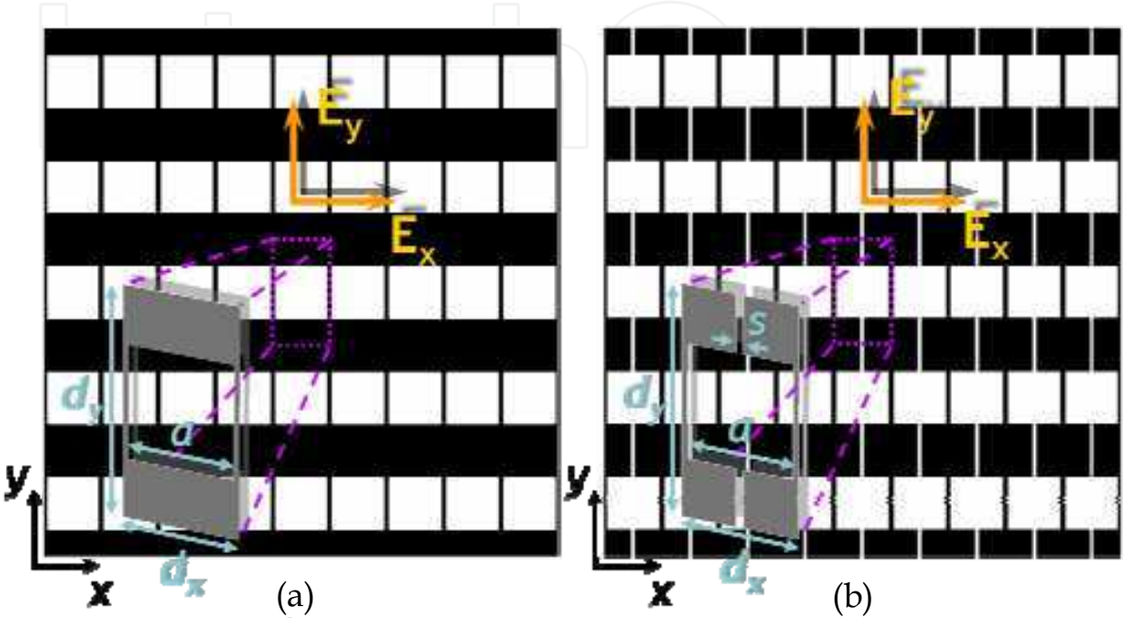

Fig. 7. Sketch of (a) doubly periodic subwavelength hole arrays, and (b) self-complementary subwavelength hole arrays. Insets: unit cell with parameters

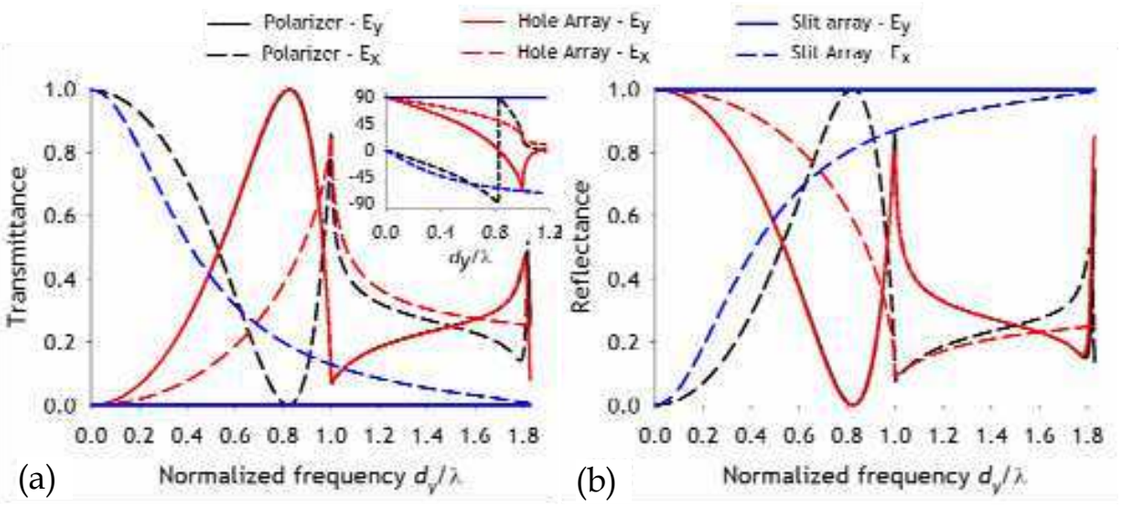

Fig. 8. Simulation results of the polarization dependent transmittance (a) and reflectance (b). Vertical, E_y, polarization and horizontal, E_x, polarization are represented by continuous and dashed traces respectively for vertical slit arrays (blue), hole array (red) and for the proposed polarizer (black). (inset) Transmittance phase

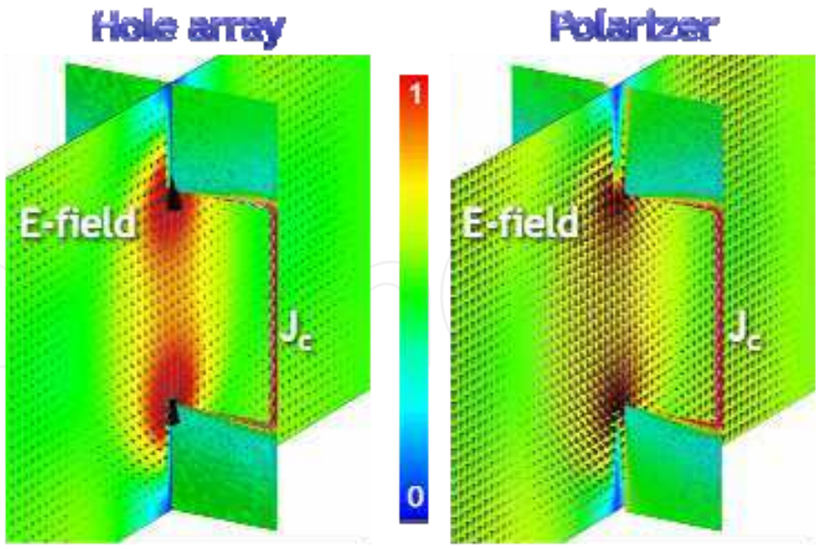

(a) (b)

Fig. 9. Plot of the conduction and displacement currents at the ET resonance with vertically polarized (E_y) wave. Hole array case (a) and polarizer (b). The E-field is depicted in a perpendicular yz-cutting plane through the middle of a hole

On the other hand, under the horizontal polarization the EM response of the self-complementary SHAs can be seen as governed by small patch arrays – which are precisely the complementary screen of the SHAs and whose spectrum presents a resonant rejection band at the ET frequency (extraordinary reflection, ER) – connected with narrow wires. Following the same preceding analysis of the current distribution we may arrive at the conclusion that, like slits connecting holes, the connecting narrow wires cause in this case a negligible perturbation on the current distribution and thus, in the response of the small patch arrays.

4.1 Equivalent circuit analysis

An alternative and more quantitative approach to explain the electromagnetic response of the self-complementary SHAs is based on lumped element equivalent circuit and high order mode excitation. This approach is founded on the reduction of the problem of a plane wave normally incident on a periodic structure to a single unit cell in an artificial waveguide (Beruete et al., 2007). When the periodic screen has symmetric elements, some transversal periodic boundary conditions can be substituted by electric or magnetic walls/symmetry planes (assuming linear polarized plane wave normal incidence). With this approach it is possible to compare the performance of ET hole arrays and ET-based polarizers, see Fig. 7.

As it is well-known, transversal electric (TE) modes below cutoff store magnetic energy, whereas transversal magnetic (TM) modes store electric energy. It is precisely this reactive character of evanescent higher order modes added to the divergence obtained at the onset of propagation that gives rise to the ET, as explained in (Beruete et a., 2007; Medina et al., 2008) and in the text below. From this platform and invoking once again Babinet's principle, the ER can also be explained.

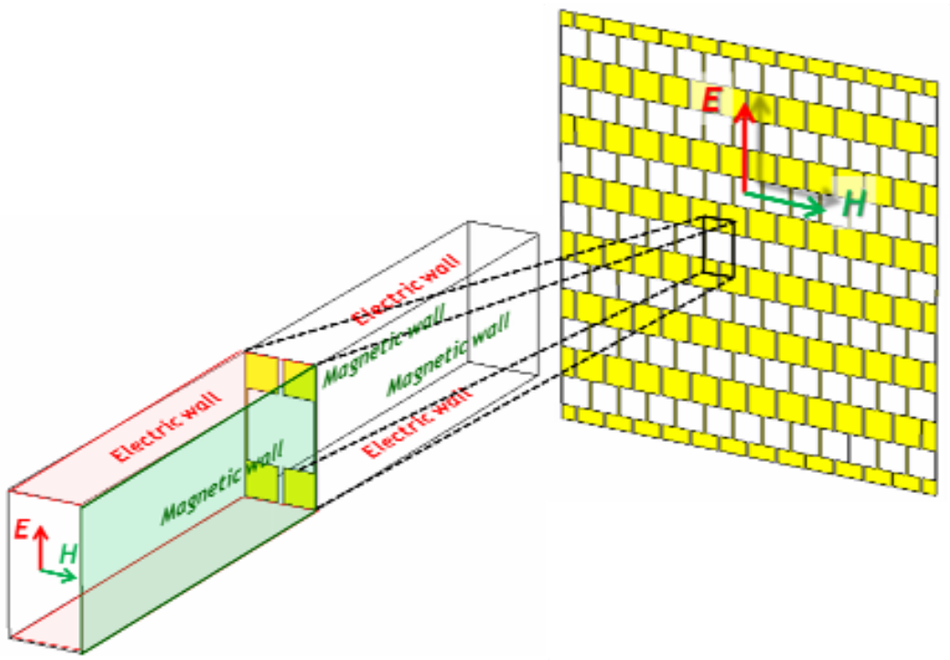

Fig. 10. Planes defining the boundary conditions of the artificial waveguide (vertical polarization)

Starting with the case of vertical polarization, where the polarizer presents an ET-like behaviour, and accepting that the slit does not fundamentally modifies the global performance, the equivalent circuit extracted for ET hole arrays (Beruete et al., 2007; Medina et al., 2008) can be applied without modification. It can be deduced from the dominant modes of the artificial waveguide. Before going to a comprehensive study of the modes, ET can be qualitatively explained using the concept of excess energy stored by evanescent modes (modes below cutoff). More specifically, applying the well-known procedure of component elimination from rotational Maxwell's equations (Jackson, 1999; Ramo et al., 1994) and imposing vertical polarization and the boundary conditions of Fig. 10, the functional expressions of the artificial waveguide modes are easily found:

- TE modes:

$$E_y(x,y) = \frac{j\omega\mu}{k_c^2}\frac{m\pi}{d_x}A^{mn}\cos\left(m\pi x/d_x\right)\cos\left(n\pi y/d_y\right) \tag{2a}$$

$$H_x(x,y) = \frac{-j\beta}{k_c^2}\frac{m\pi}{d_x}A^{mn}\cos\left(m\pi x/d_x\right)\cos\left(n\pi y/d_y\right) \tag{2b}$$

$$H_z(x,y) = A^{mn}\sin\left(m\pi x/d_x\right)\cos\left(n\pi y/d_y\right) \tag{2c}$$

- TM modes:

$$E_y(x,y) = \frac{j\beta}{k_c^2}\frac{n\pi}{d_y}B^{mn}\cos\left(m\pi x/d_x\right)\cos\left(n\pi y/d_y\right) \tag{3a}$$

$$H_x(x,y) = \frac{j\omega\varepsilon}{k_c^2}\frac{n\pi}{d_y}B^{mn}\cos(m\pi x/d_x)\cos(n\pi y/d_y) \tag{3b}$$

$$E_z(x,y) = B^{mn}\cos(m\pi x/d_x)\sin(n\pi y/d_y) \tag{3c}$$

where β is the propagation constant in the longitudinal direction, A^{mn}, B^{mn} are normalization factors that are found once the power carried by each mode is known, and k_c is the cutoff wavenumber calculated as:

$$k_c = \sqrt{\left(\frac{m\pi}{d_x}\right)^2 + \left(\frac{n\pi}{d_y}\right)^2} \tag{4}$$

The symmetry of the problem only allows for even indices: m, n = ±2, ±4, ±6, and so forth. The TEM wave is directly deduced from Eqs. 2 or 3 imposing $m = n = 0$. It is evident here that TE (TM) modes do not admit a solution with $m = 0$ ($n = 0$), because otherwise the wave vanishes. With that restriction in view, it is deduced that the lowest high-order mode of a rectangular unit cell where $d_x < d_y$ is the TM_{02} mode with a cutoff frequency $f_c = c/d_y$, where c is the speed of light in vacuum.
The TM_{02} mode has the next equivalent impedance below cutoff (Medina et al., 2008):

$$Z_{TM_{02}} = -j\eta_0\sqrt{\left(\frac{c}{d_y f}\right)^2 - 1} \tag{5}$$

where it is explicitly shown the capacitive character of the reactance, which is the fingerprint of TM modes below cutoff. From here, the equivalent capacitance can be deduced (Medina, 2008):

$$C_{TM_{02}} = \frac{A_{TM}}{2\pi f\eta_0\sqrt{\left(\frac{c}{d_y f}\right)^2 - 1}} \tag{6}$$

The small central aperture below cutoff has an inductive character, as it is well-known from the times of radar development (Collin, 1991; Ramo et al., 1994; Schwinger & Saxon, 1968). This inductance is due to the TE modes below cutoff. A crucial feature of Eq. 6 is that the capacitance of the TM_{02} mode gradually diverges as the frequency approaches the cutoff frequency ($f_c = c/d_y$) and becomes infinite exactly at cutoff. This means that at the cutoff frequency a shunt short-circuit is introduced by the central element and transmission drops to zero. Additionally, as the capacitance diverges to infinite, there must be a frequency where it exactly balances the inductance of the hole and total transmission takes place. This agrees with the fact that at c/d_y there is always a zero of transmission, known as Rayleigh-Wood anomaly in grating theory and that ET resonance happens always at a frequency slightly below that condition (Medina et al., 2008).
A parallel analysis can be done for the polarization where ER occurs. However, Babinet's principle can be invoked to obtain the propagation characteristics of an infinitely thin patch array. As it has been indicated earlier, the reflection coefficient of an infinitely thin and

lossless small patch array obtained by interchanging air and metal in the previous hole array can be obtained from those of the hole array by considering the complementary excitation after the following changes (Marqués et al., 2005):

$$cB_{hole}^{inc} = E_{patch}^{inc} \tag{7a}$$

$$E_{hole}^{inc} = -cB_{patch}^{inc} \tag{7b}$$

So, the transmission coefficient of the patch array are obtained from those of the hole array for the complementary (orthogonal) polarization and the same incidence angle through (Marqués et al., 2005):

$$t_{hole} + t_{patch} = 1 \tag{8}$$

For the sake of completeness, the modal analysis is done in the following. Here, instead of rotating the polarization, we rotate the unit cell so that the previous boundary conditions can be applied to this problem and the same mode formulation is applicable. With this modification in mind, the lowest high-order mode now is transversal electric, the TE_{20} whose cutoff frequency is $f_c = c/d_x$ (note that, as d_x and d_y have interchanged their roles with respect to the previous case, the frequency is the same as before).
The TE_{20} mode has the next equivalent admittance below cutoff (Beruete et al., 2011; Medina et al., 2008):

$$Y_{TE_{20}} = -\frac{j}{\eta_0}\sqrt{\left(\frac{c}{d_x f}\right)^2 - 1} \tag{9}$$

where it is shown the inductive character of the reactance, which is the mark of TE modes below cutoff. From here, an equivalent inductance can be deduced (Beruete et al., 2011; Medina et al., 2008):

$$L_{TE_{20}} = \frac{A_{TM}\eta_0}{2\pi f\sqrt{\left(\frac{c}{d_y f}\right)^2 - 1}} \tag{10}$$

An array of disconnected apertures such as a patch array (recall that we have found that the small channel connecting patches has no effect on the resonance) has capacitive character. Observing that Eq. 10 predicts a divergence of the inductance as the frequency approaches cutoff, then there is a frequency where it fully compensates the capacitance of the patch array. So, apparently the previous argument applies, but there is a subtle modification: now, due to Babinet's principle, the equivalent circuit is a series *LC* so that when $f = f_c$ the patch array is an open circuit, and the transmission coefficient is unity and at the frequency where inductance and capacitance are matched it is equivalent to a short circuit and there is a null in transmission.

4.2 Toward the experiment

The primary obstacle for testing self-complementary SHAs is the difficulty of producing a free-standing structure while the robustness and stiffness are kept, because there are as

many apertures as metal. To overcome this problem, the patterns were milled in the copper layer of the commercial microwave substrate ARLON CUCLAD 250 LX (metallization thickness t = 35 μm, and conductivity $\sigma_{Cu} = 5.8 \cdot 10^7$ S/m) and the structure was sandwiched between two dielectric slabs (dielectric constant ε_r = 2.43 and dielectric thickness h = 0.49 mm) to deal with symmetric geometries. Because of the dielectric embedding, the Babinet's principle is no longer entirely valid and thus, a fine tuning is required. The final in-plane periodicities of the prototype are d_x = 1.8 mm and d_y = 3.8 mm.

In Fig. 11, the simulated frequency response of a pure self-complementary structure (parameters d_x = 2.7 mm, d_y = 5.0 mm, a = 2.5 mm, s = 0.2 mm as shown on the right panel) embedded in the aforementioned dielectric slabs is shown (black traces). Apart from the fact that the ET peak/ER dip moves to 34 GHz, out of our experimental bandwidth that extends from 45 to 260 GHz, which does not diminish the generality of the following discussion, peaks and dips in the frequency response take place at different points. In general, the dielectric loading has different effects on each polarization and the structure is not necessarily self-complementary. This is due to the fact that the dielectric has a finite thickness resulting in different impedance for each polarization. Then, any structure loaded with finite dielectric slabs is not generally self-complementary (García-de-Abajo et al., 2005). Nevertheless, despite the movement from the strict scenario of Babinet's principle, we want to remark that the structure shows localized complementariness in the band of interest (ET/ER resonance) and that the principles governing the ET peak/ER dip are the same as for the ideal free-standing screen.

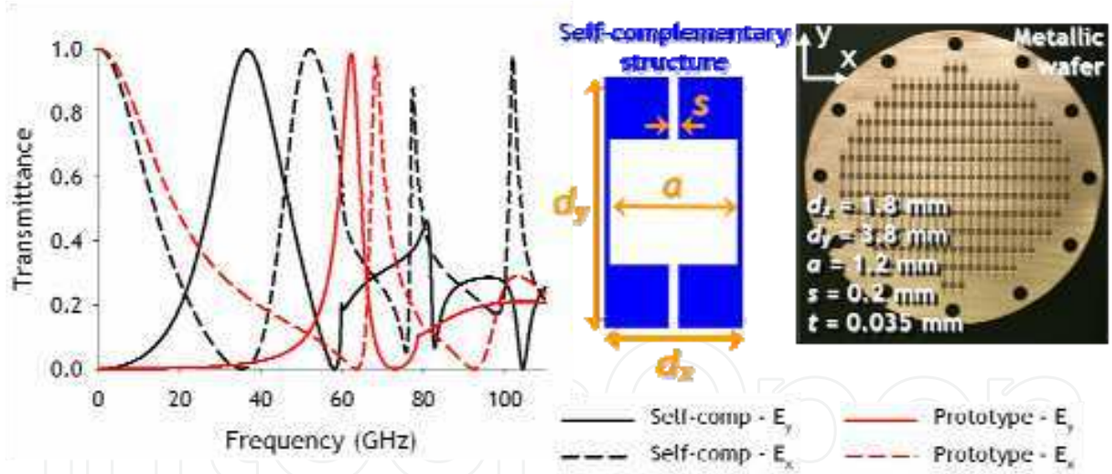

Fig. 11. (Left) Simulated polarization-dependent transmittance of self-complementary (black) and optimized (red) structures embedded in two dielectric slabs (ε_r = 2.43 and thickness of each slab h = 0.49 mm). (Right) Unit cell of a rectangular self-complementary ET polarizer with parameters: d_x = 2.7 mm, d_y = 5.0 mm, a = 2.5 mm, and s = 0.2 mm, and photograph of the fabricated prototype whose parameters are depicted in the figure

Taking the ideas of the previous paragraph into account, along with our fabrication tolerances and our interest in having the ET peak/ER dip and Wood's anomaly within our experimental bandwidth, the fine tuning of the hole array parameters leads to the final prototype shown on the right-hand side of Fig. 11, whose simulated EM response is plotted also in the graph of Fig. 11 (red lines). In addition to the desired frequency shift, note that

the peaks have become sharper mainly because the filling factor (aperture-to-unit cell area ratio) has decreased from 0.5 to 0.29.
CST Microwave Studio™ allows launching a circularly polarized wave and then, visualizing the evolution of the electric field when it passes through the polarizer screen (assuming screen of infinite extension). Thus, we take advantage of this option to illustrate in Fig. 12 the polarization filtering of the designed prototype. The incident wave is circularly polarized, but because of the strong reflection of the horizontal component, the pattern seen at the input (top right corner in each panel of Fig. 12) becomes elliptical. This is nicely manifested by comparing both t_0 and $t_0+3\Delta t$ cases, where the horizontal component, E_x, seen in $t_0+3\Delta t$ exceeds in magnitude the electric field component y, E_y, of t_0. On the other hand, the outgoing wave has an ordinary linear (vertical) polarized pattern.

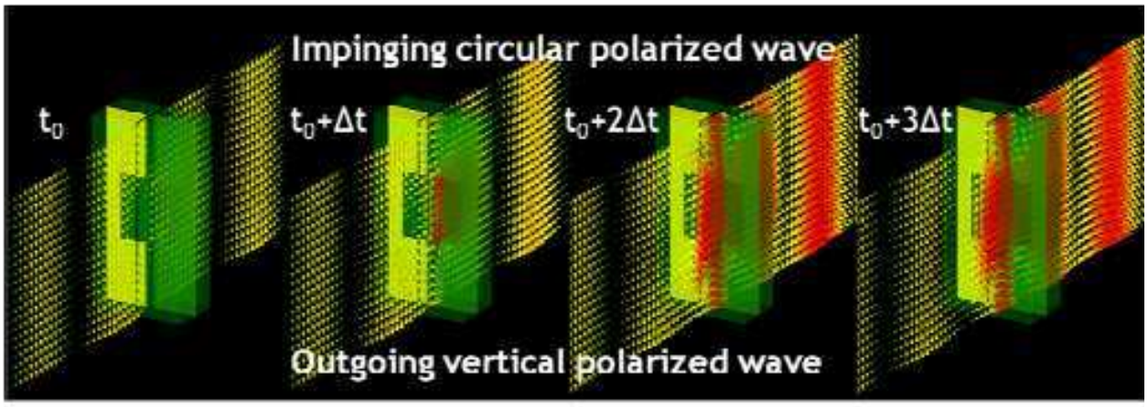

Fig. 12. Time evolution of the electric field for the self-complementary SHAs. From left to right t_0, $t_0+\Delta t$, $t_0+2\Delta t$, and $t_0+3\Delta t$

To finish with the numerical results, the effective parameters: electric permittivity ε, magnetic permeability μ and index of refraction n are retrieved from the complex scattering parameters, which is an established method for the experimental characterization of unknown materials (Ghodgaonkar et al., 1990; Nicolson & Ross, 1970). Notice that, for gratings, this is just an assignation of equivalent material parameters to a thin periodic pattern and lacks of truly physical meaning because they may be changed when several identical layers are stacked together (because of loading effect), for instance. Also, it should be noted that we adopt in this chapter a time dependence of e^{jwt}, which is followed in most engineering disciplines.
It can be shown that the scattering parameters are related to the transmission T and reflection coefficient Γ by the following equations:

$$S_{11} = \frac{\Gamma(1-T^2)}{1-\Gamma^2 T^2} = \frac{\Gamma(1-e^{-j2nk_0d})}{1-\Gamma^2 e^{-j2nk_0d}} \tag{11a}$$

$$S_{21} = \frac{T(1-\Gamma^2)}{1-\Gamma^2 T^2} = \frac{(1-\Gamma^2)e^{-jnk_0d}}{1-\Gamma^2 e^{-j2nk_0d}} \tag{11b}$$

After some mathematics it can be easily derived from these equations that:

$$z = \pm\sqrt{\frac{(1+S_{11})^2 - S_{21}^2}{(1-S_{11})^2 - S_{21}^2}} \tag{12}$$

$$n = \frac{1}{k_0 d}\left\{\left(\mathrm{Im}\left(\ln\left(e^{-jnk_0 d}\right)\right) + 2m\pi\right) + j\,\mathrm{Re}\left(\ln\left(e^{-jnk_0 d}\right)\right)\right\} \tag{13}$$

where m is an integer related to the branch index of Re(n). Finally, the electric permittivity $\varepsilon_{eff} = n/z$, and the magnetic permeability $\mu_{eff} = n \cdot z$.

The retrieved parameters are displayed in Fig. 13 at those frequencies nearby the ET peak/ER dip where the transmittance is above 0.5. The main features observed on the retrieval are:

- For E_y (vertical) polarization, the effective electric permittivity undergoes a Lorentzian-like dispersion around the ET peak arisen from the resonant character. Moreover, it comes from negative values – not appreciable in Fig. 13 – as it is expected because the structure behaves as a diluted metal (Drude dispersion) for low frequencies. The effective magnetic permeability in turn displays an anti-resonance whose origin is hypothesised to come from the finite size of the unit cell (Koschny et al., 2003). However, recently it has been associated to magneto-electric coupling (Alú, 2010, 2010b). Finally, the effective index of refraction presents a strong dispersion because of the resonant nature, reaching values from 0 up to 2.2.
- For the E_x (horizontal) polarization, the effective electric permittivity, magnetic permeability and index of refraction exhibits similar responses as for E_y, but at higher frequencies (at around Rayleigh-Wood's anomaly (just after the ER dip)). Nevertheless, it should be mentioned that the effective electric permittivity for this polarization cannot be described by a Drude dispersion for low frequencies since the structure is capacitive and supports a propagating mode at DC.

It should be noted that from the effective permittivity and permeability, we could find the parameters of the lumped elements modelling the response of the self-complementary-inspired hole array polarizer through the relationships $Z' = Z/l = j\omega\mu_0\mu_r$ and $Y' = Y/l = j\omega\varepsilon_0\varepsilon_r$, in which l is assumed to be the effective length of the slab. Nevertheless, this is left as an exercise for the reader.

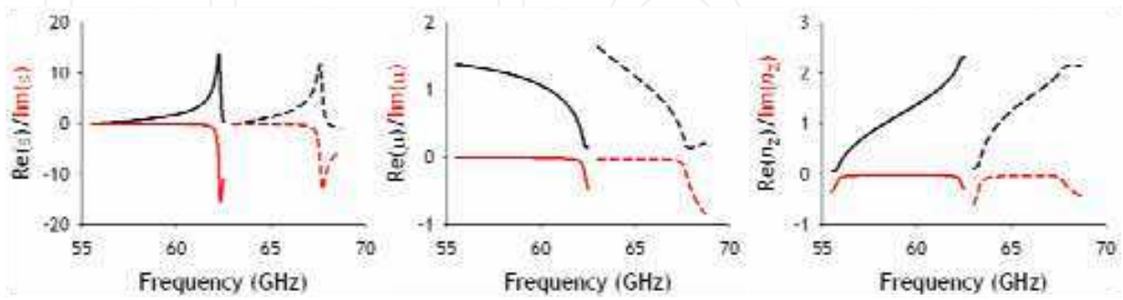

Fig. 13. From left to right: effective electric permittivity, magnetic permeability, and index of refraction. Solid and dashed lines account for E_y (vertical) and E_x (horizontal) polarization, respectively. Black and red lines represent real and imaginary part of the aforementioned constitutive parameters, respectively. The values are only computed within the -3 dB pass-band

Measurements were performed under Fresnel illumination with the AB-Millimetre™ quasi-optical (QO) vector network analyzer by using a QO bench, see Fig. 14. The AB-Millimetre™ is an all-solid-state electronics which generates millimetre-submillimetre waves by frequency multiplication, and detects them by harmonic mixing. The QO setup consists of a corrugated horn antenna that generates a very well linearly polarized Gaussian beam which, after two ellipsoidal mirrors, is focused over the sample under test with a beamwaist of around 28 mm at the frequencies of this work. There, the transmitted and reflected beams are obtained. The transmitted beam passes through another pair of identical mirrors and reaches the receiver antenna. This antenna is another corrugated horn well matched to the Gaussian beam.

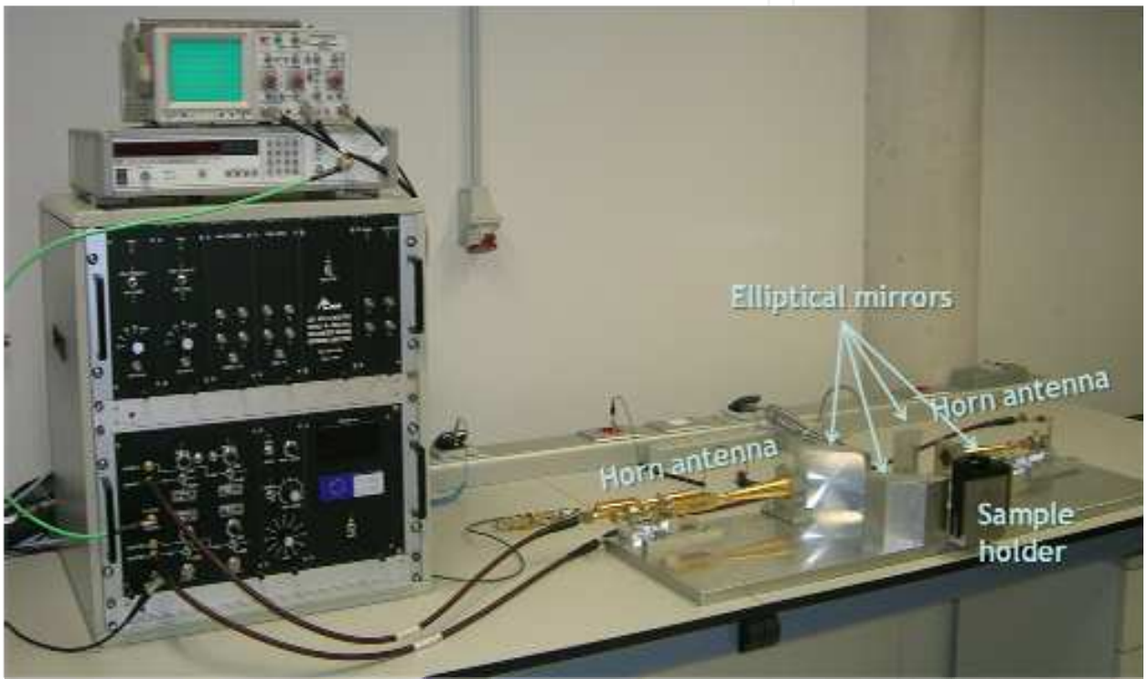

Fig. 14. Photograph of the experimental setup

The experimental results are shown in the black curves of Fig. 15 for the transmission [Fig. 15(a)] and reflection [Fig. 15(b)]. Both vertical polarization, E_y (solid lines), and the orthogonal, E_x (dashed lines) are measured. For incident E_y, a clear resonance around 61 GHz is detected with practically total transmission (0.95), followed by a second relative maximum at 74 GHz (0.12) related to the symmetric distribution of the surface waves at each interface (Kuznetsov et al., 2009) and the null corresponding to the Rayleigh–Wood's anomaly at around 79 GHz. The orthogonal level at 61 GHz is 0.029, whereas it reaches 0.002 at 63 GHz where the power intensity peak of E_y is still above 0.9. Notice also that at 69 GHz, the horizontal polarization achieves a transmittance of 0.81 while the vertical is 0.06, indicating that at this frequency we have as a by-product a polarization filtering behaviour too (for the orthogonal polarization).

As it is anticipated from the nearby Babinet's scenario, there is a relatively good complementary correspondence between the transmission and reflection measured results. The best we can expect with the given dielectric loaded structure is having the peak of

transmission and the dip of reflection of the orthogonal components at almost the same frequency.

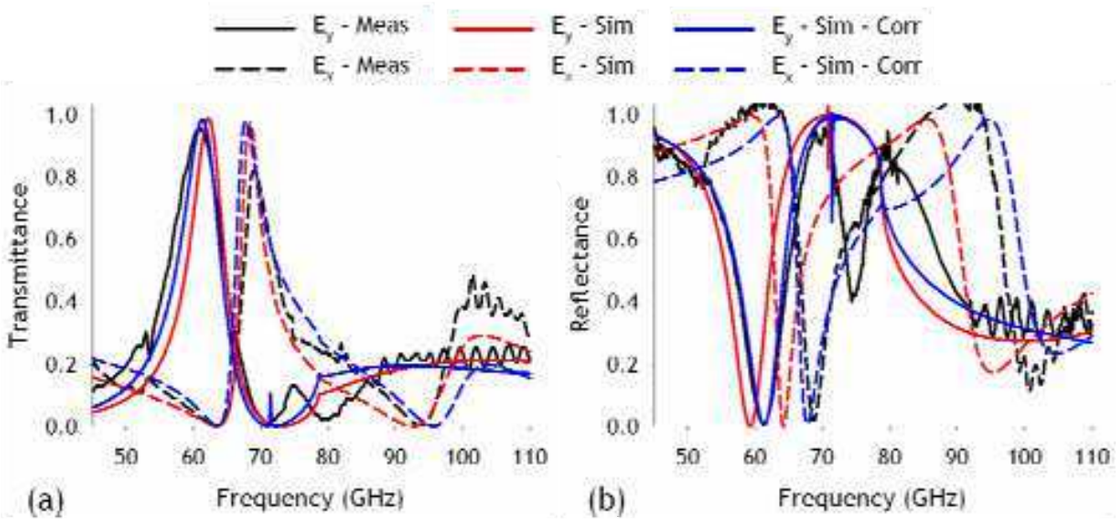

Fig. 15. Measurement (black) and simulation results of the prototype (red) and the prototype with an assembly defect modelled by an air slab of 0.1 mm between the perforated plate and one of the dielectric slabs (blue). Solid trace for E_y and dashed one for E_x: (a) Transmission spectrum for E_y and E_x and (b) Idem for reflection

Figure 15 renders also the numerical results given by CST Microwave Studio™ when the problem is treated as an infinite screen and under an ideal plane wave illumination, see red traces. Despite all the differences between the experimental setup (finite structure and Gaussian beam illumination to name the more prominent) and the simulation, the peak/dip positions and magnitudes are in reasonable agreement. To further approximate to the real problem, we have also explored numerically the possibility that the dielectric slab position is no longer ideal. The motivation of this study emerged after carefully analysing the manufacture and assembly procedures: firstly, the pattern is etched in one of the copper layer of ARLON CUCLAD 250 LX, whereas the other is removed; secondly, both metal layers of another wafer of ARLON are removed; finally, the single dielectric slab is screwed to the previous dielectric-backed metal pattern. Therefore, these steps permit only to ensure perfect contact between the metal layer with one of the dielectric slabs and good contact in the frame of the wafer with the other dielectric slab (see photograph of the prototype in Fig. 11, where there are 12 circular holes on the framework of the wafer for the screwing), but not at the centre. Then, a thin air layer is susceptible of existing between the metal and one slab. To account for this potential imperfection, we have included an air slab of 0.1 mm between the perforated plate and one of the dielectric slabs. The numerical results are shown by blue traces in Fig. 15 and they corroborate that the manufacture process can be the origin of the non-idealities measured.

The results presented up to now confirm the hypothesis of self-complementary structures as a guide method for designing dielectric embedded structures. Had it been a single plate metallic free-standing polarizer, the response would have been similar to the theoretical curves of Fig. 8.

5. Stacked self-complementariness-based extraordinary transmission layers

The next question to be answered is whether the subwavelength-stacking of these modified SHAs would still lead to backward wave propagation (effective negative refractive index) for the vertical polarization as it happens for the fishnet-like metamaterial (Beruete et al., 2006; Dolling et al., 2006; Zhang et al., 2005b). And also, whether the propagation of the horizontal polarization would be inhibited as it happens for the single layer configuration. To answer these question one should recall that Babinet's principle applies for infinitely thin metallic layers, as it was explained in section 3. Thus, the multi-layering of self-complementary extraordinary transmission layers leads certainly to backward wave propagation, but does not have to fulfil Babinet. Therefore, the direct stack of the previous prototypes may or may not arrive at a linear polarizer exhibiting effective negative refractive index. Nevertheless, the authors showed in a previous work that by a smart design one can positively have such linear polarizer (Beruete et al., 2007b).

We can further play around with the unit cell dimensions, and by a new clever design, overlap the first mode of each polarization, leading to a birefringent medium, where the ET axis behaves as an effective negative refractive index and the orthogonal axis as an effective positive refractive index (Beruete et al., 2008).

Here, we investigate in more detail this last design by constructing a wedge, which is a common geometrical approach to check the value of the effective index of refraction of a metamaterial (Navarro-Cía et al., 2008). If the stack behaves indeed as a single negative birefringent medium, one polarization undergoes negative refraction, whereas the orthogonal has positive refraction.

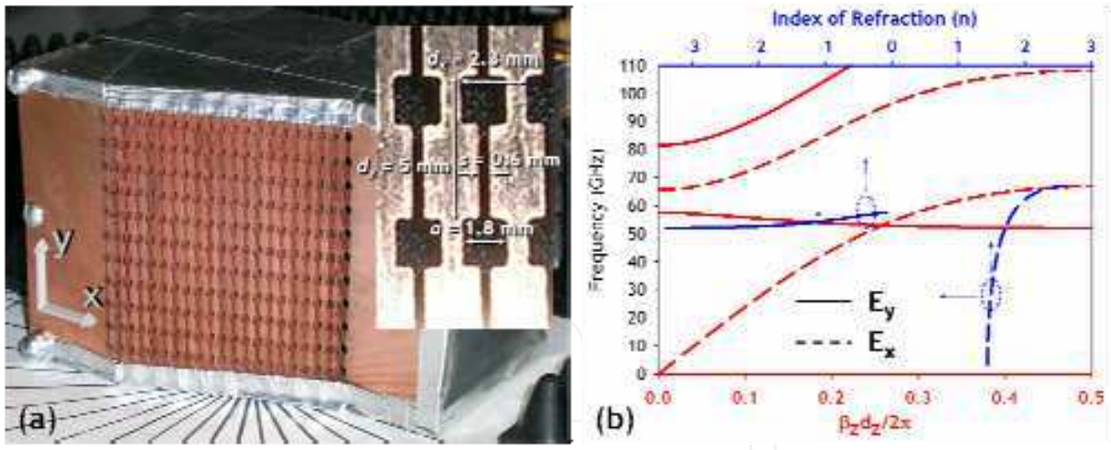

Fig. 16. (a) Picture of the prototype whose angle is 20.28 deg. (b) Dispersion diagram (red curve) and index of refraction (blue curve) – for the first propagating modes – calculated numerically for the infinite stack; solid lines correspond to electric field impinging vertically (E_y), whereas dashed lines represent the response under horizontal polarization (E_x); dotted blue arrows indicate the corresponding axes to the curve

To check this supposition, a prism made of modified SHAs was manufactured (Beruete et al., 2010; Navarro-Cía et al., 2010). A picture of the prototype and zoom-in of the unit cell whose parameters are: transversal periodicities d_x = 2.3 mm, d_y = 5 mm, longitudinal periodicity d_z = 0.85 mm, hole size a = 1.8 mm, slit width s = 0.6 mm and metal (copper)

thickness w = 0.35 mm; are shown in Fig. 16(a). The effective zone of the wedge comprises 21 slits (and the corresponding number of lines of holes) and 11 horizontal rows, which means a 55 mm × 48.3 mm size. On the other hand, the prism has total dimensions of 91 mm × 65 mm × 65 mm/45 mm (width × height × length).

As we have done in previous works (Beruete et al., 2006, 2006b, 2007, 2007b, 2007c, 2008, 2010; Navarro-Cía et al., 2008, 2010), our assumptions in the stack's properties rely on the dispersion diagram. In this case, the dispersion diagram of our present prism is plotted in Fig. 16(b), along with the index of refraction associated to each first couple of propagation modes (one corresponds to vertical polarization, E_y, whereas the other to the orthogonal one, E_x). Notice that in the frequency range between 52 and 57.5 GHz, an overlap of effective negative and positive refractive index propagation modes is expected.

The experimental setup is similar to the one used in preceding works (Beruete et al., 2010; Navarro-Cía et al. 2008, 2010). In short, the prism is illuminated from the back by a corrugated horn antenna and the outgoing beam deflection is scanned at a distance z = 400 mm by another identical corrugated horn antenna. Both antennas are connected to the AB-Millimetre™ QO vector network analyzer. The frequency band and effective aperture used impose that we are dealing with near field or Fresnel zone due to the fact that $2 \cdot D^2/\lambda \approx 1100$ mm, where D is the largest dimension of the prism (Balanis, 2005). The calibration or reference is done by using a face to face antennas configuration.

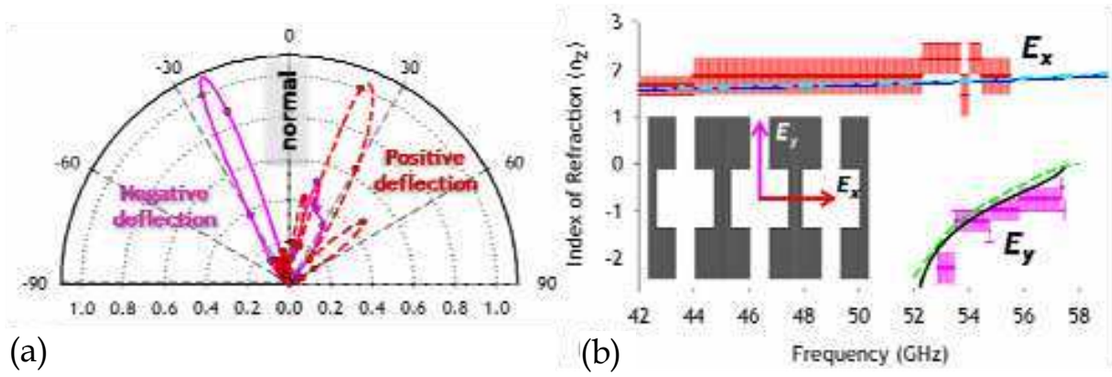

Fig. 17. (a) Angular power distribution normalized to its maximum for both polarizations at 53.8 GHz. The spots correspond to the measurement results, whereas the curves are a smooth interpolation. (b) Evolution of the refractive index as a function of the frequency for both polarizations. Red and pink spots are the experimental points along with the corresponding error bars, the blue and black, and cyan and green curves are the equivalent simulation results derived from the dispersion diagram and from the standard S-parameter method respectively for each polarization

Figure 17(a) shows undoubtedly the negative and positive deflection experienced by the vertical and horizontal polarized beam respectively at 53.8 GHz, whereas Fig. 17(b) displays a quantitative comparison between numerical and experimental results in terms of effective index of refraction. There, the effective index of refraction derived from the experimental results via Snell's law for both polarizations alongside the experimental error bars are plotted, and the index computed with CST Microwave Studio™ by two different methods are also shown superimposed. Solid lines account for the effective index of refraction derived from the dispersion diagram, whereas dashed lines define the effective index of

refraction retrieved from the S-parameters (Ghodgaonkar et al., 1990; Nicolson & Ross, 1970). In the latter procedure, the metal has been modelled by copper and 10 stacked layers have been considered as a representative number of stacked layers of the real prototype. Remarkable is the good agreement between numerical and experimental results despite the fact already pointed out regarding near-field measurement and finite structure.

6. Conclusion

The EM properties of SHAs arranged in rectangular lattice can be enhanced by applying Babinet's concepts. Indeed, by inserting vertical subwavelength slit arrays connecting holes, a self-complementary structure is obtained whose EM response in terms of transmittance and reflectance fulfil Babinet's principle. This feature leads to a perfect linear polarizer: the vertical polarization undergoes ET (total transmission in the lossless case), whereas the orthogonal polarization exhibits extraordinary reflection (total reflection in the lossless case) at the same frequency. The qualitatively explanation founded on Babinet's principle has been complemented with a description based on lumped element equivalent circuit and high order mode excitation. Furthermore, an inversion technique has been used to retrieve the effective constitutive EM parameters (effective electric permittivity, effective magnetic permeability and effective index of refraction) that model the response of the grating. In addition, the induced surface currents as well as the electric field evolution through the grating have been represented to pedagogically support the conclusions derived from Babinet's principle and self-complementariness. As a natural extension, it has been analysed briefly the propagation behaviour of stacked self-complementariness-based ET layers. It has been shown that for a certain design parameters it is possible to have an effective birefringent medium whose vertical and horizontal axis behaves as an effective negative and positive refractive index, respectively. Finally, the theoretical and numerical analyses for single- and multi-layer have been confirmed experimentally at millimetre-waves.

7. Acknowledgment

We wish to thank a whole host of our friends and colleagues for many useful discussions. They are Dr. Igor Campillo, Universidad de Deusto, Spain; Dr. Francisco Falcone, Universidad Pública de Navarra, Spain; Professor Vitaliy Lomakin, University of California San Diego, United States; and Dr. Philippe Goy, AB Millimetre, France.
Work supported by Spanish Government under contract Consolider "ENGINEERING METAMATERIALS" CSD2008-00066.

8. References

Alú, A. (December 2010). First-Principle Homogenization Theory for Periodic Metamaterial Arrays, In: *arXiv,* Available from: http://arxiv.org/abs/1012.1351

Alú, A. (December 2010). Restoring the Physical Meaning of Metamaterial Constitutive Parameters, In: *arXiv,* Available from: http://arxiv.org/abs/1012.1353

Balanis, C.A. (2005). *Antenna Theory Analysis and Design,* Wiley-Interscience, ISBN 978-047-1667-82-7, Hoboken (NJ), USA

Barnes, W.L., Murray, W.A., Dintinger, J., Devaux, E., & Ebbesen, T.W. (2004). Surface plasmon polaritons and their role in the enhanced transmission of light through periodic arrays of subwavelength holes in a metal film, *Physical Review Letters,* Vol. 92, No. 10, (March 2004), pp. 107401-1-4

Beruete, M., Sorolla, M., Campillo, I., Dolado, J.S., Martín-Moreno, L., Bravo-Abad, J., & García-Vidal, F.J. (2004). Enhanced millimetre-wave transmission through subwavelength hole arrays, *Optics Letters,* Vol. 29, No. 21, (November 2004), pp. 2500-2502

Beruete, M., Campillo, I., Dolado, J.S., Rodríguez-Seco, J.E., Pere, E., & Sorolla, M. (2004b). Enhanced microwave transmission and beaming using a subwavelength slot in corrugated plate, *IEEE Antennas and Wireless Propagation Letters,* Vol. 3, No. 16, (December 2004), pp. 328-331

Beruete, M., Sorolla, M., Campillo, I., & Dolado, J.S. (2005). Subwavelength slotted Corrugated plate with enhanced quasioptical millimeter wave transmission, *IEEE Microwave and Wireless Components Letters,* Vol. 15, No. 4, (April 2005), pp. 286-288

Beruete, M., Sorolla, M., & Campillo, I. (2006). Left-handed extraordinary optical transmission through a photonic crystal of subwavelength hole arrays, *Optics Express,* Vol. 14, No. 12, (June 2006), pp. 5445-5455

Beruete, M. (2006b). *Millimeter-Wave Extraordinary Transmission: Connection to Metamaterials and Technological Applications*, Doctoral thesis

Beruete, M., Campillo, I., Navarro-Cía, M., Falcone, F., & Sorolla, M. (2007). Molding Left- or Right-Handed Metamaterials by Stacked Cut-Off Metallic Hole Arrays, *IEEE Transactions on Antennas and Propagation, Special issue in honour or Prof. L.B. Felsen,* Vol. 55, No. 6, (June 2007), pp. 1514-1521

Beruete, M., Navarro-Cía, M., Sorolla, M., & Campillo, I. (2007b). Polarized left-handed extraordinary optical transmission of subterahertz waves, *Optics Express,* Vol. 15, No. 13, (June 2007), pp. 8125-8134

Beruete, M., Navarro-Cía, M., Campillo, I., Goy, P., & Sorolla, M. (2007c). Quasioptical Polarizer Based on Self-Complementary Sub-Wavelength Hole Arrays, *IEEE Microwave and Wireless Components Letters,* Vol. 17, No. 12, (December 2007), pp. 834-836

Beruete, M., Navarro-Cía, M., Sorolla, M., & Campillo, I. (2008). Polarization selection with stacked hole array metamaterial, *Journal of Applied Physics,* Vol. 103, No. 5, (March 2008), pp. 053102-1-4

Beruete, M., Navarro-Cía, M., Falcone, F., Campillo, I., & Sorolla, M. (2010). Single negative birefringence in stacked spoof plasmon metasurfaces by prism experiment, *Optics Letters,* Vol. 35, No. 5, (March 2010), pp. 643-645

Beruete, M., Navarro-Cía, M., Kuznetsov, S.A., & Sorolla, M. (2011). Circuit approach to the minimal configuration of terahertz anomalous extraordinary transmission, *Applied Physics Letters,* Vol. 98, No. 1, (January 2011), pp. 014106-1-3

Bethe, H.A. (1944). Theory of diffraction by small holes, *Physical Review,* Vol. 66, No. 7-8, (October 1944), pp. 163-182

Betzig, R.E., Lewis, A., Harootunian, A., Isaacson, M., & Kratschmer, E. (1986). Near-field scanning optical microscopy (NSOM): Development and Biophysical Applications, *Biophysical Journal,* Vol. 49, No. 1, (January 1986), pp. 269-279

Betzig, R.E., (1988). *Nondestructive optical imaging of surfaces with 500 angstrom resolution,* Doctoral thesis

Born, M. & Wolf, E. (1999). *Principles of Optics: Electromagnetic Theory of Propagation, Interference and Diffraction of Light,* Cambridge University Press, ISBN 978-052-1642-22-4, Cambridge, UK

Bouwkamp, C.J. (1950). On Bethe's theory of diffraction by small holes, *Philips Research Reports,* Vol. 5, No. 5, (1950), pp. 321-332

Bouwkamp, C.J. (1950b). On the diffraction of electromagnetic waves by small circular disks and holes, *Physical Review,* Vol. 5, No. 6, (1950), pp. 401-422

Bouwkamp, C.J. (1954). Diffraction theory, *Reports on Progress in Physics,* Vol. 17, No. 1, (January 1954), pp. 35-100

Brown, J. (1953). Artificial dielectric having refractive indices less than unity, *Proceedings of the IEE,* Vol. 100, No. 5, (October 1953), pp. 51-62

Chen, C.C. (1971). Diffraction of electromagnetic waves by a conducting screen perforated periodically with circular holes, *IEEE Transactions on Microwave Theory and Techniques,* Vol. 19, No. 5, (May 1971), pp. 475-481

Chen, C.C. (1973). Transmission of microwave through perforated flat plates of finite thickness, *IEEE Transactions on Microwave Theory and Techniques,* Vol. 21, No. 1, (January 1973), pp. 1-7

Collin, R.E. (1991). *Field Theory of Guided Waves,* Wiley-IEEE Press, ISBN 978-087-9422-37-0, Piscataway (NJ), USA

Degiron, A., Lezec, H.J., Barnes, W.L., & Ebbesen, T.W. (2002). Effects of hole depth on enhanced light transmission through subwavelength hole arrays, *Applied Physics Letters,* Vol. 81, No. 23, (October 2002), pp. 4327- 4329

Dolling, G., Enkrich, C., Wegener, M., Soukoulis, C.M., & S. Linden. (2006). Simultaneous negative phase and group velocity of light in a metamaterial, *Science,* Vol. 312, No. 5775, (May 2006), pp. 892- 894

Ebbesen, T.W., Lezec, H.J., Ghaemi, H., Thio, T., & Wolf, P.A. (1998). Extraordinary optical transmission through sub-wavelength hole arrays, *Science,* Vol. 391, No. 6668, (February 1998), pp. 667-669

Falcone, F., Lopetegi, T., Laso, M.A.G., Baena, J.D., Bonache, J., Beruete, M., Marqués, R., Martín, F., & Sorolla, M. (2004). Babinet principle applied to metasurface and metamaterial design, *Physical Review Letters,* Vol. 93, No. 19, (November 2004), pp. 197401-1-4

Fano, U. (1941). The theory of anomalous diffraction grating and of quasistationary waves on metallic surfaces (Sommerfield's waves), *Journal of Optical Society of America,* Vol. 31, No. 3, (March 1941), pp. 213-222

García-de-Abajo, F.J., Gómez-Medina, R., & Sáenz, J.J. (2005). Full transmission through perfect-conductor subwavelength hole arrays, *Physical Review E,* Vol. 72, No. 1, (July 2005), pp. 016608-1-4

García-Vidal, F.J., Lezec, H.J., Ebbesen, T.W., & Martín-Moreno, L. (2003). Multiple paths to enhance optical transmission through a single subwavelength slit, *Physical Review Letters,* Vol. 90, No. 21, (May 2003), pp. 213901-1-4

García-Vidal, F.J., Martín-Moreno, L., & Pendry, J.B. (2005). Surfaces with holes in them: new plasmonic metamaterials, *Journal of Optics A: Pure and Applied Optics,* Vol. 7, No. 2, (January 2005), pp. S97-S101

Genet, C., van Exter, M.P., & Woerdman, J.P. (2003). Fano-type interpretation of red shifts and red tails in hole array transmission spectra, *Optics Communications,* Vol. 225, No. 4-6, (October 2003), pp. 331-336

Ghaemi, H.F., Thio, T., Grupp, D.E., Ebbesen, T.W., & Lezec, H.J. (1998). Surface plasmons enhance optical transmission through sub-wavelength holes, *Physical Review B,* Vol. 58, No. 11, (September 1998), pp. 6779-6782

Ghodgaonkar, D.K., Varadan, V.V., & Varadan, V.K. (1990). Free-Space Measurement of Complex Permittivity and Complex Permeability of Magnetic Materials at Microwave Frequencies, *IEEE Transactions on Instrumentation and Measurements,* Vol. 39, No. 2, (April 1990), pp. 387-394

Goldsmith, P.F. (1998). *Quasioptical Systems: Gaussian Beam, Quasioptical Propagation, and Applications,* Wiley-IEEE Press, ISBN 978-078-0334-39-7, Piscataway (NJ), USA

Grupp, D.E., Lezec, H.J., Thio, T., & Ebbesen, T.W. (1999). Beyond the Bethe limit: Tunable enhanced light transmission through a single subwavelength aperture. *Advanced Materials,* Vol. 11, No. 10, (July 1999), pp. 860-862

Hessel, A. & Oliner A.A. (1965). A new theory of Wood's anomalies on optical gratings. *Applied Optics,* Vol. 4, No. 10, (October 1965), pp. 1275-1297

Ishimaru, A. (1990). *Electromagnetic Wave Propagation, Radiation, and Scattering,* Prentice hall, ISBN 978-013-2490-53-5, Boston, USA

Jackson, J.D. (1999). *Classical Electrodynamics,* John Wiley & Sons, ISBN 978-047-1309-32-1, New York, USA

Jackson, D.R., Oliner, A.A., Zhao, T., & Williams, J.T. (2005). The beaming of light at broadside through a subwavelength hole: Leaky-wave model and open stopband effect. *Radio Science,* Vol. 40, No. 6, (September 2005), pp. 1-7

Koschny, Th, Markos, P., Smith, D.R., & Soukoulis, C.M. (2001). Resonant and antiresonant frequency dependence of the effective parameters of metamaterials. *Physical Review E,* Vol. 68, No. 6, (December 2003), pp. 065602-1-4

Krishnan, A., Thio, T., Kim, T.J., Lezec, H.J., Ebbesen, T.W., Wolff, P.A., Pendry, J.B., Martín-Moreno, L., & García-Vidal, F.J. (2001). Evanescently coupled resonance in surface plasmon enhanced transmission. *Optics Communications,* Vol. 200, No. 1-6, (October 2001), pp. 1-7

Kuznetsov, S.A., Navarro-Cía, M., Kubarev, V.V., Gelfand, A.V., Beruete, M., Campillo, I., & Sorolla, M. (2009). Regular and anomalous Extraordinary Optical Transmission at the THz-gap. *Optics Express,* Vol. 17, No. 14, (July 2009), pp. 11730-11738

Lezec, H.J., Degiron, A., Deveaux, E., Linke, R.A., Martín-Moreno, L., García-Vidal, F.J., & Ebbesen, T.W. (2002). Beaming light from a sub-wavelength aperture. *Science,* Vol. 297, No. 5582, (August 2002), pp. 820-822

Lezec, H.J., & Thio, T. (2004). Diffracted evanescent wave model for enhanced and suppressed optical transmission through subwavelength hole arrays. *Optics Express,* Vol. 12, No. 16, (August 2004), pp. 3629-3651

Lomakin, V., Chen, N.W., Li, S.Q., & Michielssen, E. (2004). Enhanced transmission through two-period arrays of sub-wavelength holes. *IEEE Microwave and Wireless Components Letters,* Vol. 14, No. 7, (July 2004), pp. 355-357

Lomakin, V., & Thio, T. (2005). Enhanced transmission through metallic plates perforated by arrays of subwavelength holes and sandwiched between dielectric slabs. *Physical Review B,* Vol. 71, No. 23, (June 2005), pp. 235117-1-10

Marqués, R., Baena, J.D., Beruete, M., Falcone, F., Lopetegi, T., Sorolla, M., Martín, F., & García, J. (2005). Ab initio Analysis of Frequency Selective Surfaces Based on Conventional and Complementary Split Ring resonators. *Journal of Optics A: Pure and Applied Optics,* Vol. 7, No. 2, (January 2005), pp. S38-S43

Martín-Moreno, L., García-Vidal, F.J., Lezec, H.J., Pellerin, K.M., Thio, T., Pendry, J.B., & Ebbesen, T.W. (2001). Theory of extraordinary optical transmission through subwavelength hole arrays. *Physical Review Letters,* Vol. 86, No. 6, (February 2001), pp. 1114-1117

Medina, F., Mesa, F., & Marqués, R. (2008). Extraordinary Transmission Through Arrays of Electrically Small Holes From a Circuit Theory Perspective, *IEEE Transactions on Microwave Theory and Techniques,* Vol. 56, No. 12, (December 2008), pp. 3108-3120

Medina, F., Ruiz-Cruz, J.A., Mesa, F., Rebollar, J.M., Montejo-Garai, J.R., & Marqués, R. (2009). Experimental verification of extraordinary transmission without surface plasmons, *Applied Physics Letters,* Vol. 95, No. 7, (August 2009), pp. 071102-1-3

Mumcu, G., Sertel, K., & Volakis, J.L. (2006). Miniature antennas and arrays embedded within magnetic photonic crystals, *IEEE Antennas and Wireless Propagation Letters,* Vol. 5, No. 1, (December 2006), pp. 168-171

Navarro-Cía, M., Beruete, M., Sorolla, M., & Campillo, I. (2008). Negative refraction in a prism made of stacked subwavelength hole arrays. *Optics Express,* Vol. 16, No. 2, (January 2008), pp. 560-566

Navarro-Cía, M., Beruete, M., Falcone, F., Sorolla, M., & Campillo, I. (2010). Polarization-tunable negative or positive refraction in self-complementariness-based extraordinary transmission prism. *Progress In Electromagnetics Research,* Vol. 103, (April 2010), pp. 101-114

Nicolson, A.M., & Ross, G.F. (1970). Measurement of the Intrinsic Properties of Materials by Time-Domain Techniques, *IEEE Transactions on Instrumentation and Measurements,* Vol. 19, No. 4, (November 1970), pp. 377-382

Notomi, M. (2002). Negative refraction in photonic crystals, *Optical and Quantum Electronics,* Vol. 34, No. 1-3, (January 2002), pp. 133-143

Pendry, J.B., Martín-Moreno, L., & García-Vidal, F.J. (2004). Mimicking surface plasmons with structured surfaces. *Science,* Vol. 305, No. 5685, (August 2004), pp. 847-848

Porto, J.A., García-Vidal, F.J., & Pendry, J.B. (1999). Transmission resonances on metallic gratings with very narrow slits. *Physical Review Letters,* Vol. 83, No. 14, (October 1999), pp. 2845-2848

Ramo, S., Whinnery, J.R., & Van Duzer, T. (1994). *Fields and Waves in Communication Electronics,* John Wiley & Sons, ISBN 978-047-1585-51-3, New York, USA

Rayleigh, Lord (1907). On the dynamical theory of gratings. *Proceedings of the Royal Society of London A,* Vol. 79, No. 532, (August 2007), pp. 399-416

Robinson, L.A. (1960). Electrical properties of metal-loaded radomes. *Wright air Develop. Div. Rep. WADD-TR-60-84,* Vol. 60-84, (February 1960), pp. 1-114

Salomon, L., Grillot, F.D., Zayats, A.V., & de Fornel, F. (2001). Near-field distribution of optical transmission of periodic subwavelength holes in a metal film, *Physical Review Letters,* Vol. 86, No. 6, (February 2001), pp. 1110- 1113

Sarrazin, M., Vigneron, J.P., & Vigoureux, J.M. (2003). Role of Wood anomalies in optical properties of thin metallic films with a bidimensional array of subwavelength holes, *Physical Review B,* Vol. 67, No. 8, (February 2003), pp. 085415-1-8

Sarrazin, & M., Vigneron, J.P. (2005). Light transmission assisted by Brewster-Zenneck modes in chromium films carrying a subwavelength hole array, *Physical Review B,* Vol. 71, No. 7, (February 2005), pp. 075404-1-5

Schröter, U., & Heitmann, D. (1998). Surface-plasmon enhanced transmission through metallic gratings, *Physical Review B,* Vol. 58, No. 23, (December 1998), pp. 15419-15421

Schwinger, J., & Saxon, D. (1968). *Discontinuities In Waveguides – Notes on Lectures by Julian Schwinger,* Gordon and Breach, ISBN 978-067-7018-40-9, New York, USA

Synge, E.H. (1928). A suggested model for extending microscopic resolution into the ultra-microscopic region, *Philosophical Magazine,* Vol. 6, No. 35, (August 1928), pp. 356-362

Thio, T., Pellerin, K.M., Linke, R.A., Ebbesen, T.W., & Lezec, H.J. (2001). Enhanced light transmission through a single sub-wavelength aperture, *Optics Letters,* Vol. 26, No. 24, (December 2001), pp. 1972-1974

Thio, T., Lezec, H.J., Ebbesen, T.W., Pellerin, K.M., Lewen, G.D., Nahata, A., Linke, R.A. (2002). Giant optical transmission of sub-wavelength apertures: physics and applications, *Nanotechnology,* Vol. 13, No. 3, (June 2002), pp. 429-432

Treacy, M.M.J. (1999). Dynamical diffraction in metallic optical gratings, *Applied Physics Letters,* Vol. 75, No. 5, (June 1999), pp. 606-608

Treacy, M.M.J. (2002). Dynamical diffraction explanation of the anomalous transmission of light through metallic gratings, *Physical Review B,* Vol. 66, No. 19, (November 2002), pp. 195105-1-11

Ulrich, R. (1967). Far-infrared properties of metallic mesh and its complementary structure, *Infrared Physics,* Vol. 7, No. 1, (March 1967), pp. 37-55

Ulrich, R., & Tacke, M. (1972). Submillimeter waveguide on periodic metal structure, *Applied Physics Letters,* Vol. 22, No. 5, (March 1973), pp. 251-253

Ulrich, R. (1974). Modes of propagation on an open periodic waveguide for the far infrared, *Proceedings of Symposium Optical and Acoustical Microelectronics,* pp. 359-376, New York, USA, April 16-18, 1974

Wood, R.W. (1902). On a remarkable case of uneven distribution of light in a diffraction grating spectrum, *Proceedings of the Physical Society of London,* Vol. 18, No. 1, (June 1902), pp. 269-275

Ye, Y.H., & Zhang, J.Y. (2005). Enhanced light transmission through cascaded metal films perforated with periodic hole arrays, *Optics Letters,* Vol. 30, No. 12, (June 2005), pp. 1521-1523

Zhang, S., Fan, W., Malloy, K.J., & Brueck, S.R.J. (2005). Near-infrared double negative metamaterials, *Optics Express,* Vol. 13, No. 13, (June 2005), pp. 4922-4930

Zhang, S., Fan, W., Panoiu, N.C., Malloy, K.J., Osgood, R.M., & Brueck, S.R.J. (2005b). Experimental demonstration of near-infrared negative-index metamaterials, *Physical Review Letters,* Vol. 95, No. 13, (September 2005), pp. 137404-1-4

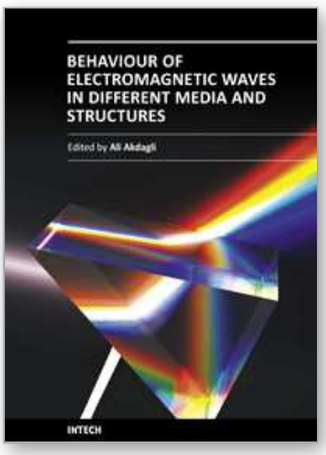

Behaviour of Electromagnetic Waves in Different Media and Structures

Edited by Prof. Ali Akdagli

ISBN 978-953-307-302-6
Hard cover, 440 pages
Publisher InTech
Published online 09, June, 2011
Published in print edition June, 2011

This comprehensive volume thoroughly covers wave propagation behaviors and computational techniques for electromagnetic waves in different complex media. The chapter authors describe powerful and sophisticated analytic and numerical methods to solve their specific electromagnetic problems for complex media and geometries as well. This book will be of interest to electromagnetics and microwave engineers, physicists and scientists.

How to reference

In order to correctly reference this scholarly work, feel free to copy and paste the following:

Miguel Navarro-Cía, Miguel Beruete and Mario Sorolla (2011). Electromagnetic Response of Extraordinary Transmission Plates Inspired on Babinet's Principle, Behaviour of Electromagnetic Waves in Different Media and Structures, Prof. Ali Akdagli (Ed.), ISBN: 978-953-307-302-6, InTech, Available from: http://www.intechopen.com/books/behavior-of-electromagnetic-waves-in-different-media-and-structures/electromagnetic-response-of-extraordinary-transmission-plates-inspired-on-babinet-s-principle1

INTECH
open science | open minds

InTech Europe
University Campus STeP Ri
Slavka Krautzeka 83/A
51000 Rijeka, Croatia
Phone: +385 (51) 770 447
Fax: +385 (51) 686 166
www.intechopen.com

InTech China
Unit 405, Office Block, Hotel Equatorial Shanghai
No.65, Yan An Road (West), Shanghai, 200040, China
中国上海市延安西路65号上海国际贵都大饭店办公楼405单元
Phone: +86-21-62489820
Fax: +86-21-62489821

IntechOpen